Since January 2020 Elsevier has created a COVID-19 resource centre with free information in English and Mandarin on the novel coronavirus COVID-19. The COVID-19 resource centre is hosted on Elsevier Connect, the company's public news and information website.

Biosensors and Bioelectronics 223 (2023) 115025

Contents lists available at ScienceDirect

Biosensors and Bioelectronics

journal homepage: www.elsevier.com/locate/bios

Programmable DNA biocomputing circuits for rapid and intelligent screening of SARS-CoV-2 variants

Fang Deng [a,b,1], Jiafeng Pan [a,b,1], Zhi Liu [b], Lingwen Zeng [c,d], Junhua Chen [a,*]

[a] National-Regional Joint Engineering Research Center for Soil Pollution Control and Remediation in South China, Guangdong Key Laboratory of Integrated Agro-environmental Pollution Control and Management, Institute of Eco-environmental and Soil Sciences, Guangdong Academy of Sciences, Guangzhou, 510650, China
[b] College of Bioscience and Biotechnology, Hunan Agricultural University, Changsha, 410128, China
[c] Guangdong Langyuan Biotechnology Co., LTD, Foshan, 528313, China
[d] School of Food Science and Engineering, Foshan University, Foshan, 528231, China

ARTICLE INFO

Keywords:
Logic gate
Biocomputing circuit
Molecular switch
Intelligent screening
COVID-19
SARS-CoV-2 variant

ABSTRACT

The frequent emergence of SARS-CoV-2 variants increased viral transmissibility and reduced protection afforded by vaccines. The rapid, multichannel, and intelligent screening of variants is critical to minimizing community transmissions. DNA molecular logic gates have attracted wide attention in recent years due to the powerful information processing capabilities and molecular data biocomputing functions. In this work, some molecular switches (MSs) were connected with each other to implement arbitrary binary functions by emulating the threshold switching of MOS transistors and the decision tree model. Using specific sequences of different SARS-CoV-2 variants as inputs, the MSs net was used to build several molecular biocomputing circuits, including NOT, AND, OR, INHIBIT, XOR, half adder, half subtractor, full adder, and full subtractor. Four fluorophores (FAM, Cy3, ROX, and Cy5) were employed in the logic systems to realize the multichannel monitoring of the logic operation results. The logic response is fast and can be finished with 10 min, which facilitates the rapid wide-population screening for SARS-CoV-2 variants. Importantly, the logic results can be directly observed by the naked eye under a portable UV lamp, thus providing a simple and intelligent method to enable high-frequency point-of-care diagnostics, particularly in low-resource communities.

1. Introduction

The coronavirus disease of 2019 (COVID-19) pandemic caused by severe acute respiratory syndrome coronavirus 2 (SARS-CoV-2) poses a great threat and burden to the global public health (Li et al., 2021; Wang et al., 2020a; Zhou et al., 2020). Currently, the surge of various SARS-CoV-2 variants, such as Beta (B.1.351), Delta (B.1.617.2), Omicron (B.1.1.529), and so forth, have displayed high infectivity and spreading speed (Bai et al., 2021; Han et al., 2022; Rockett et al., 2022; Yang et al., 2022). The outbreaks of multifarious variants increased the infection and reinfection risk and reduced the protections provided by vaccines or neutralizing antibodies (Moitra et al., 2022; Sun et al., 2022; Suzuki et al., 2022; Syeda et al., 2022). The development of multiplex sensing platform that can quickly and accurately detect SARS-CoV-2 variants can effectively stop the spread of COVID-19 (Erdem et al., 2022; Rodriguez et al., 2021; Valera et al., 2021; Zhang et al., 2022). The reverse transcription polymerase chain reaction (RT-PCR) technique is widely used to detect pathogen nucleic acids and is considered as a gold standard in infectious disease diagnostics because of its high sensitivity and specificity (Yao et al., 2021). However, it requires expensive equipment, skilled technicians, and time-consuming procedures, which are not appropriate for the point-of-care (POC) molecular diagnosis of different SARS-CoV-2 variants. The CRISPR sensing system, which has attracted much attention in recent years (Feng et al., 2021; Kaminski et al., 2021; Rahimi et al., 2021), is still unable to meet the needs of the detection of different variant due to the requirement of PAM region and gRNA (Liang et al., 2022; Wang et al., 2021; Xiong et al., 2021). Thus, there is still a great demand to design a simple, fast, and intelligent sensing platform that can realize the multiple detection of SARS-CoV-2 variants (Cyranoski, 2021).

Based on threshold switches and binary operations, Metal-Oxide-Semiconductor (MOS) can perform predefined logic functions and

* Corresponding author.
E-mail address: 222chenjunhua@163.com (J. Chen).
[1] These two authors contributed equally to this work.

https://doi.org/10.1016/j.bios.2022.115025
Received 24 September 2022; Received in revised form 5 December 2022; Accepted 16 December 2022
Available online 18 December 2022

computing tasks (Dai et al., 2021; Hao et al., 2022; Lee et al., 2011). MOS transistors are widely used as the building blocks in modern electronics. In order to perform the digital computing at the molecular level, DNA molecule can be used as fundamental logic circuit elements to replace MOS transistors (Arter et al., 2020; Song et al., 2019; Su et al., 2019; Wang et al., 2020b). Through modular molecular design and programmable reaction dynamics, DNA logic circuits can realize the biocomputing with excellent scalability and good accuracy (Cai et al., 2022; Chen et al., 2012, 2018, 2021; Feng et al., 2020; Gong et al., 2019; Zhang et al., 2020). However, there are some limitations in the expansion of the molecular circuit. For example, (I) Typical scale-up approaches were just a simple stack of basic logic gates, which increased the amounts of DNA strands that might induce cross reactions (Garg et al., 2018; Ge et al., 2016). (II) As the NOT logic gate produced ON signals before receiving the output of its upstream gate, this circuit might generate a false output (Qian and Winfree, 2011).

In the present work, we addressed these challenges by developing a DNA molecular biocomputing system. Through emulating the threshold switching of MOS transistors and the decision tree model (Goswami et al., 2021), six interconnected molecular switches (MSs) were developed to execute multiple arithmetic functions. Importantly, this molecular computing system has been successfully applied to the multichannel intelligent detection of SARS-CoV-2 and several variants, including Beta (B.1.351), Delta (B.1.617.2), Kappa (B.1.617.1), Lambda (C.37), and Omicron (B.1.1.529). This molecular biocomputing system not only holds great potential for developing a large-scale complex DNA computer system, but also can serve as a public health screening tool to distinguish specific SARS-CoV-2 variants in environmental and clinical samples.

2. Materials and methods

2.1. Materials

DNA probes were ordered from Shanghai Sangon Biotechnology Co., Ltd. (Shanghai, China) and the sequences were listed in Table S1 (Supporting Information). All unlabeled DNA probes were ULTRAPAGE purified and all labeled strands were HPLC purified by Shanghai Sangon Biotechnology Co., Ltd. (Shanghai, China). All used sequences are marked with specific colors, which match the colors in the schematic illustration. All DNA sequences were designed to minimize undesired interactions using NUPACK (http://www.nupack.org/).

2.2. Bioinformatics analysis

Full-genome sequences of SARS-CoV-2 and variants were downloaded from GISAID (https://www.gisaid.org/) and GenBank (http://www.ncbi.nlm.nih.gov/genbank/). Phylogenetic trees were inferred using MEGA6 software. Through analysis of phylogenetic results and full-genomic sequence alignment (Figs. S1 and S2, Supporting Information), we obtained the specific sequences of SARS-CoV-2, Beta variant (EPI_ISL_1254583), Delta variant (EPI_ISL_3140302), Kappa variant (EPI_ISL_2304115), Lambda variant (EPI_ISL_3333569), and Omicron (EPI_ISL_6704867). The DNA sequences of A1, A0, B1, B0, C1, and C0 were selected as the specific sequences of SARS-CoV-2, Beta (B.1.351), Delta (B.1.617.2), Kappa (B.1.617.1), Lambda (C.37), and Omicron (B.1.1.529) variants, respectively (Fig. S3, Supporting Information).

2.3. Preparation of the switch molecules and reporter molecules

The powder of oligonucleotides was dissolved in 20 mM Tris-HCl buffer (pH 7.5, 140 mM NaCl, 5 mM KCl). To prepare the S(1) molecule, S(1)-1 and S(1)-2 were mixed with the molar ratio of 1:1.2 and then heated to 95 °C for 5 min and slowly cooled down to room temperature. The concentration of S(1)-1 is 200 nM. The S(2)-S(4) molecules and all reporter molecules were prepared as the same as the S(2) molecule. To prepare the S(5) molecule, the S(5)-1, S(5)-2, and S(5)-3 were mixed with the molar ratio of 1.1:1:1.5 and then heated to 95 °C for 5 min and slowly cooled down to room temperature. The concentration of S(5)-1 is 200 nM. The S(6)-S(24) molecule were prepared as the same as the S(5) molecule.

2.4. Performing computation of DNA devices

In each experiment, the input, switch molecule, and reporter molecule were mixed at room temperature. The input strand and reporter molecule were at 2.5 × concentration, where 1 × was 100 nM. The switch molecule was 2 × concentration. The fluorescence responses were carried out on the SpectraMax i3x (Molecular Devices) for 10 min with fluorescence measurements taken every 30 s. The colorimetric responses were observed by the naked eye under UV light and the photos were taken with an iPhone equipped with a wide camera.

2.5. Polyacrylamide gel electrophoresis (PAGE) analysis

10% PAGE gel was prepared for electrophoresis analysis. First, 5 μL DNA samples were mixed with 1 μL 6 × loading buffer to obtain the loading sample. Subsequently, the electrophoresis experiments were carried out at 45 V for 90 min in 1 × TBE (Tris-Borate-EDTA) buffer (pH 8.0). Finally, the PAGE gel was stained in diluted SYBR Green solution, and then photographed in a gel image system (Bio-Rad, Singapore).

3. Results and discussion

3.1. Design of molecular switch and NOT logic gate

First, we designed two MSs (switch 1 and switch 2) based on DNA strand displacement reactions, to emulate P-channel metal oxide semiconductor (PMOS) and N-channel metal oxide semiconductor (NMOS) devices (Fig. 1a and b). A1 and A0 serving as switching signals are defined as input 1 and input 0, respectively. A1 is the specific SARS-CoV-2 sequence. A0 is the specific SARS-CoV-2 Beta variant (B.1.351) sequence. The switch 1 responds to A1 and the switch 2 responds to A0. Each MS contains a double-stranded DNA switch (S(1) and S(2)). X domain in the DNA switch was used to receive the input signals (A1 and A0). Y domain in the DNA switch was used to interact with the reporter probes (R(1) and R(2)). In the presence of input A1, A1 will hybridize with the toehold 1 (domain a) to initiate the toehold-mediated strand displacement (TMSD) to liberate the S(1)-2 strand (Fig. 1c). The free S(1)-2 strand can then launch another TMSD to interact with the reporter probes R(1). The separation of FAM and BHQ1 will give out a high fluorescence signal and the switch 1 jumped from OFF to ON state. We define the threshold as 1.2X, where X is the background fluorescence intensity without target (Fig. S4, Supporting Information). We tested the switch 1 by the addition of A1 and A0, respectively. The switch responds very quickly and can be finished within 4 min (Fig. 1d). The input of A1 generated a high fluorescence signal and the input of A0 generated a low fluorescence signal (Fig. 1e). Similarly, the switch 2 can realize the transition using A0 as the input (Fig. 1f). The Cy3 output signals about the switch 2 operations were shown in Fig. 1g and h. The fluorescence intensity of the logic system toward different concentrations of target was also tested (Fig. S5, Supporting Information). The sensitivity of the logic system will not be affected by the viral load. In our logic biosensor, a high viral load can generate a high fluorescence intensity and a low viral load will generate a low fluorescence intensity. So, we can distinguish different periods of the SARS-CoV-2 infection (Cevik et al., 2021) by measuring the fluorescence intensity of the logic system.

By exchanging the Y domains of the two molecular switches and connecting them in parallel, we successfully assembled a NOT logic gate based on the complementary metal oxide semiconductor (CMOS) inverter (Hao et al., 2022; Lee et al., 2011). As shown in Fig. 2a–c, the reporter probe R(2) was used in switch 1 and the reporter probe R(1)

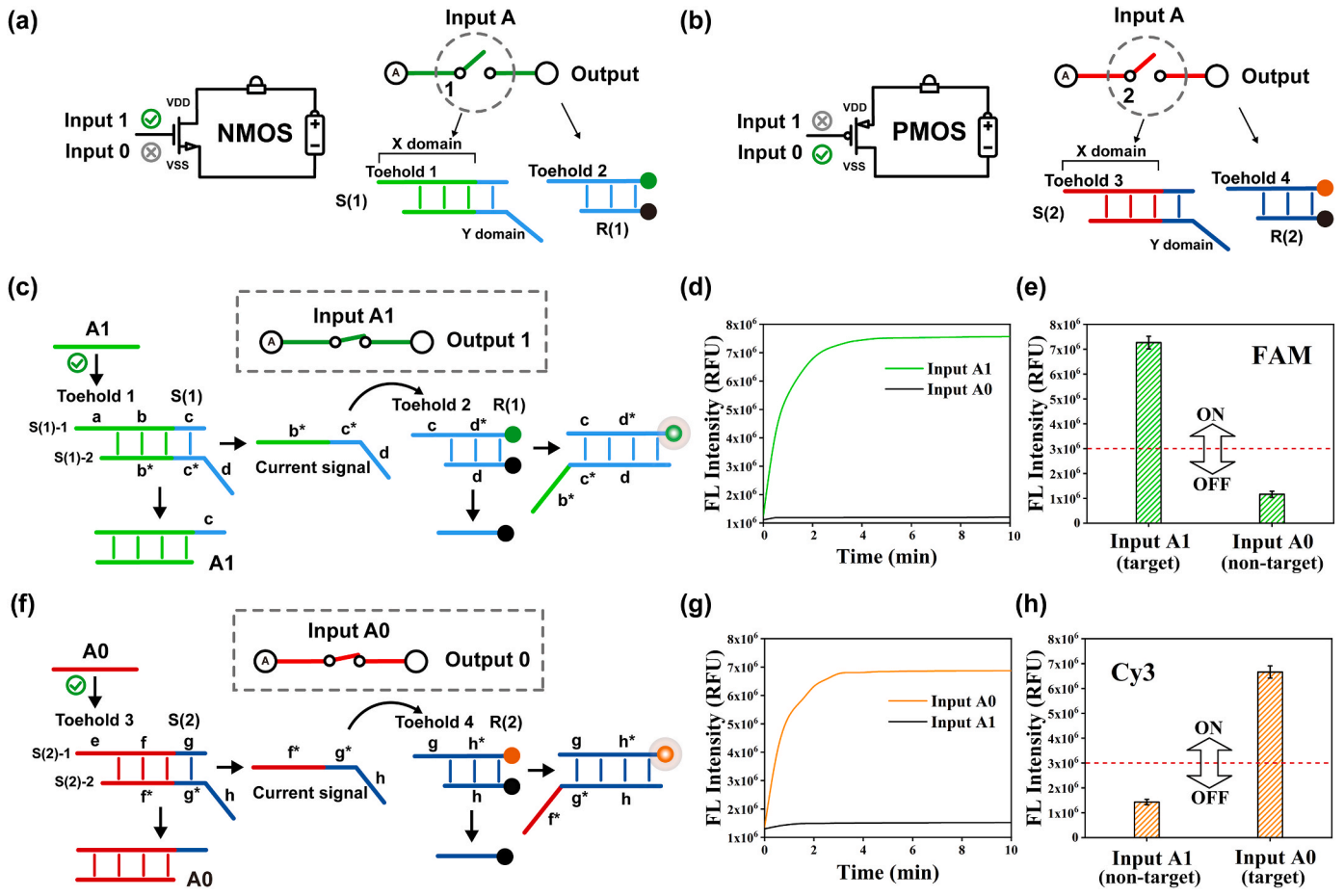

Fig. 1. Construction of molecular switch based on NMOS and PMOS and their performances. (a) Principle of NMOS and molecular details of switch 1. (b) Principle of PMOS and molecular details of switch 2. (c) Schematic illustration of switch 1 using A1 as the input. (d) Fluorescence kinetics data of switch 1. (e) Histogram shows the fluorescence signals (FAM) recorded in switch 1. The red dashed line shows the threshold value of 3.0×10^6. (f) Schematic illustration of switch 2 using A0 as the input. (g) Fluorescence kinetics data of switch 2. (h) Histogram shows the fluorescence signals (Cy3) recorded in switch 2. The red dashed line shows the threshold value of 3.0×10^6.

was used in switch 2. The presence of A1 was defined as an input 1 and the presence of A0 was defined as an input 0. We defined a high FAM fluorescence signal (green fluorescence color) as an output 1 and the Cy3 fluorescence signal (orange fluorescence color) as an output 0. The output signals can be visualized by the naked eye under UV light transilluminators or quantified by a microplate reader (Fig. 2d). In the presence of A1, the in-tube orange fluorescence color and Cy3 fluorescence signal can be observed (output = 0). In the presence of A0, the in-tube green fluorescence color and FAM fluorescence signal can be observed (output = 1) (Fig. 2e,f,h). According to the fluorescence-time curve (Fig. 2g), the toehold-mediated strand displacement reactions in the NOT logic gate can be completed within 4 min. Further prolonged the time will not increase the response signals. Thus, we can conclude that our designed NOT logic gate can be finished within 4 min. Compared with some previously reported SARS-CoV-2 sensors, our designed logic system also displayed fast response time (Table S2, Supporting Information). Those results indicated the successful construction of a NOT logic gate.

3.2. Construction of basic logic gates by molecular switch

In addition to switch 1 and switch 2, we also constructed two other MSs (switch 3 and switch 4) to respond to switching signals B1 and B0, respectively. B1 is the specific SARS-CoV-2 Delta variant (B.1.617.2) sequence. B0 is the specific SARS-CoV-2 Kappa variant (B.1.351) sequence. The switch 1 is connected with the switch 3 through designing a dual-switches S(5) (Fig. S7a, Supporting Information). The presence of A1 will displace S(5)-3 and expose the toehold 5. Then, B1 can activate the switch 3 and displace S(5)-2 to interact with R(1) for producing a FAM fluorescence signal (Fig. S7b, Supporting Information). Similarly, we connected switch 2 and switch 4 to design another dual-switches S(6) (Fig. S7c, Supporting Information). In the presence of A0 and B0, the switch flips from OFF to ON state and generates a Cy3 fluorescence signal (Fig. S7d, Supporting Information). The PAGE experiments were carried out to verify the feasibility of the dual-switches S(5) (Fig. S6, Supporting Information).

With the programmability of the DNA strands, MSs can be integrated to implement multiple logical tasks. We explored the switch assembly to perform a AND logic gate (Fig. S7e, Supporting Information). We created a programmable switch net based on the decision tree model, in which the connection between adjacent switches is configurable. Figs. S7e and f (Supporting Information) show the electronic circuit and decision tree model of a AND logic gate. Fig. S8 (Supporting Information) shows the details of the DNA reaction process of the AND logic gate. The high FAM fluorescence was defined as an output of 1 and the Cy3 fluorescence was defined as an output of 0. The presence of A1 or B1 was defined as an input 1 and the presence of A0 or B0 was defined as an input 0. The input combinations of (0,0), (0,1), and (1,0) will generate a Cy3 fluorescence. The (1,1) input combination generates a FAM fluorescence. By rearranging the molecular switch, we also constructed a OR logic gate (Figs. S7g and h), an INHIBIT logic gate (Figs. S7i and j), and a XOR logic gate (Fig. S7k,l). The corresponding details of the DNA

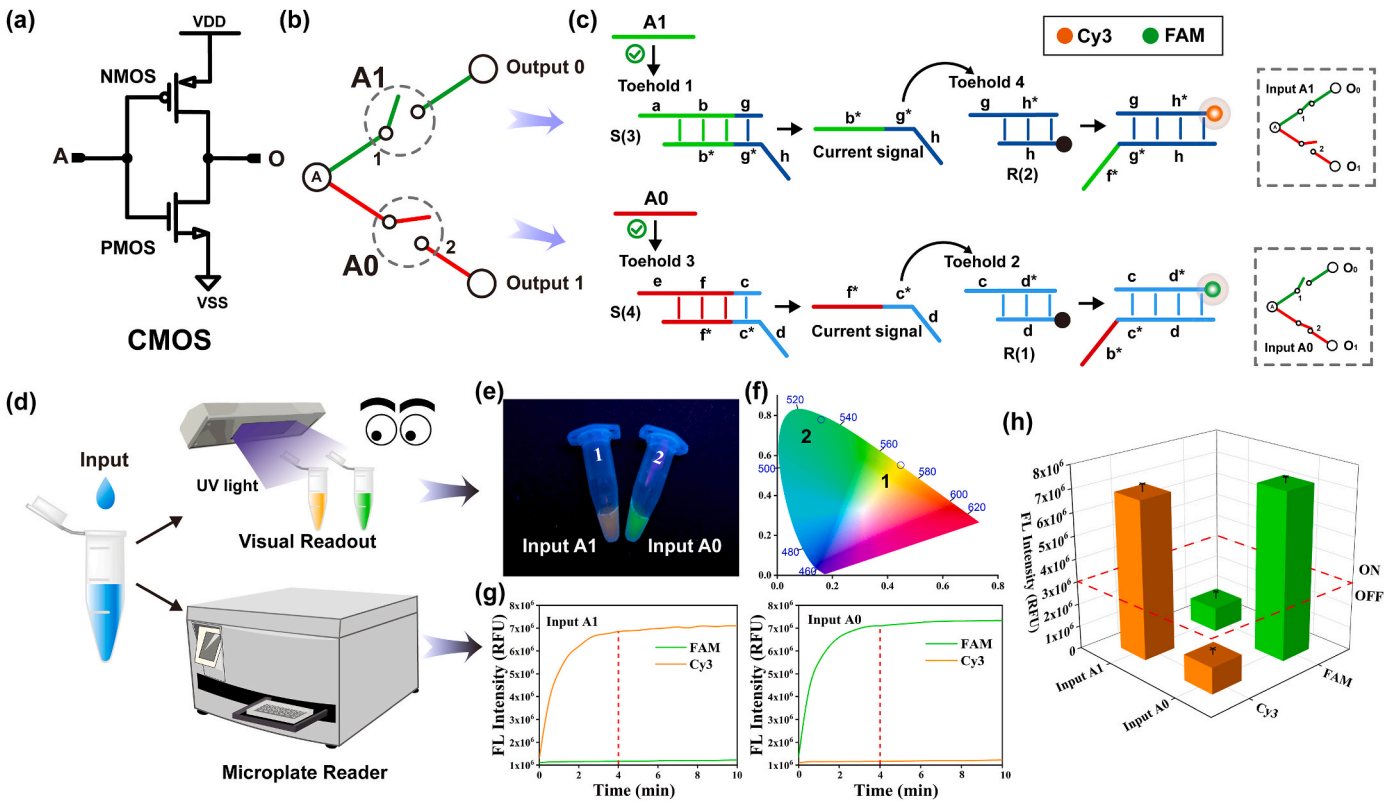

Fig. 2. Construction of a NOT logic gate and its performances. (a, b) Structure of CMOS and NOT logic gate. (c) Reaction details of the NOT logic gate. (d) Two ways to record the computation results. (e, f) The colorimetric responses of the NOT logic gate. (g) Fluorescence kinetics data of the NOT logic gate. (h) Histogram shows the fluorescence signals (Cy3 and FAM) recorded in the NOT logic gate. The red dashed line shows the threshold value of 3.0×10^6. The threshold value was about 1.2 times of the background signal.

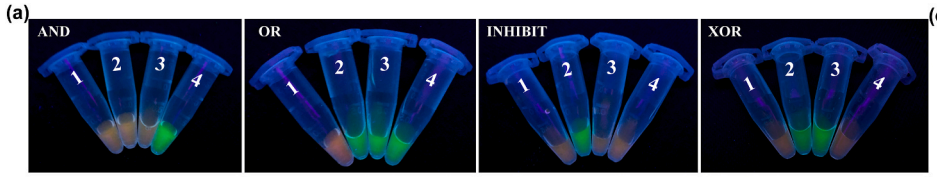

(c)

		AND	OR	INHIBIT	XOR
Input		Output			
A	B	Fluorescence			
0	0	0 (Cy3●)	0 (Cy3●)	0 (Cy3●)	0 (Cy3●)
0	1	0 (Cy3●)	1 (FAM●)	1 (FAM●)	1 (FAM●)
1	0	0 (Cy3●)	1 (FAM●)	0 (Cy3●)	1 (FAM●)
1	1	1 (FAM●)	1 (FAM●)	0 (Cy3●)	0 (Cy3●)

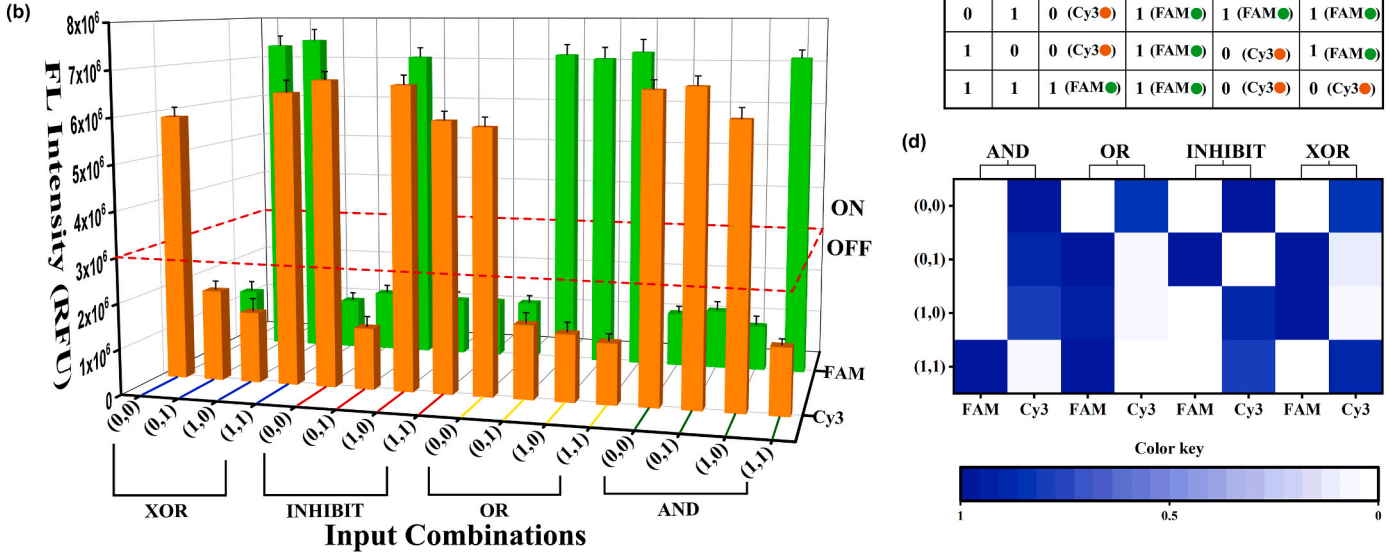

Fig. 3. Results of MSs net to implement the logic functions. (a) Fluorescence colors of the four basic logic gates (AND, OR, INHIBIT, and XOR) constructed from MSs net (the tubes 1–4 of each logic gate represent the input combinations of (0,0), (0,1), (1,0), and (1,1), respectively). (b) Histogram shows the fluorescence intensities of the four logic gates. The red dashed line shows the threshold value of 3.0×10^6. (c) Truth table of the four basic logic gates. (d) Heat map of logic fluorescence signals.

reaction processes were shown in Figs. S9, S10, and S11 (Supporting Information), respectively. The results of the four logic gates were shown in Fig. 3a,b,d. The truth table of the basic logic gates was shown in Fig. 3c. The fluorescence kinetics data of the four basic logic gates were shown in Fig. S12 (Supporting Information). In AND, OR, INHIBIT and XOR logic gates, the (1,0) or (0,1) state corresponds to one variant. We used two variants to define the (1,1) state, in which the inputs can be collected from a large infected population, in which two different SARS-CoV-2 variants may coexist.

To investigate the specificity of the logic system, we used a AND logic gate as an example to test the logic responses toward different inputs. A non-target chain (NTC) and another two SARS-CoV-2 variants were examined (C1 and C0). C1 is the specific SARS-CoV-2 Lambda (C.37) variant sequence. C0 is the specific SARS-CoV-2 Omicron (B.1.1.529) sequence. As shown in Fig. S13a (Supporting Information), A1B1 can produce a high FAM fluorescence signal. A1B0, A0B1, and A0B0 can produce a high Cy3 fluorescence signal (Fig. S13b, Supporting Information). Other input combinations involved C1, C0, and NTC failed to produce FAM or Cy3 fluorescence signals. Those results indicated the high specificity of the logic system (Fig. S13c, Supporting Information).

3.3. Construction of half adder and half subtractor

In order to construct a half adder with compact DNA configuration, three reporters (R(1), R (2), and R(3)) modified with three fluorophores (FAM, Cy3, and Cy5) were used (Fig. S14a, Supporting Information). The high FAM fluorescence signal is defined as an output of (1,0), indicating that the CARRY (C) output is 1 and the SUM (S) output is 0. The high Cy3 fluorescence signal is defined as an output of (0,1), indicating that the CARRY (C) output is 0 and the SUM (S) output is 1. The high Cy5 fluorescence signal is defined as an output of (0,0), indicating that the CARRY (C) output is 0 and the SUM (S) output is 0. In the half adder operation, a AND logic gate was used to carry out the CARRY bit function and a XOR logic gate was used to carry out the SUM bit function. The logic circuit of the half adder was shown in Fig. 4a. The details of the DNA reaction process were shown in Fig. S14b (Supporting Information). The results of the half adder were shown in Fig. 4b,d. The (0,0) input combination (A0B0) produces a high Cy5 fluorescence signal. The (0,1) and (1,0) input combinations (A0B1 and A1B0) produce a high Cy3 fluorescence signal. The (1,1) input combination (A1B1) produces a high FAM fluorescence signal. The truth table was shown in Fig. 4c. The heat map of the half adder results was shown in Fig. 4e. The circuit diagram of the half adder was shown in Fig. S16a (Supporting Information). The fluorescence kinetics data of the half adder were shown Fig. S16c (Supporting Information). The response of the half adder is rapid and can be finished within 6 min. We used the half adder logic gate as an example to test the mixture containing different variants. When different input signal molecules are present in input A or input B, there will be multiple pathways in the molecular switch network, resulting in multiple fluorescent signal outputs (Fig. S17a, Supporting Information). For instance, the current signal will be transmitted to R(1) and R(2) in the presence of input of A1, B1, and B0, and produces a high FAM and Cy3 fluorescence signal. At the same time, the current signal cannot be transmitted to R(3), thus, only a weak Cy5 fluorescence signal can be obtained (Figs. S17b–e, Supporting Information). The above results show that the logic system is capable of screening for SARS-CoV-2 variants in a wide-population and complex environmental samples.

Three reporters (R(2), R(3), and R(4)) modified with three fluorophores (Cy3, Cy5, and ROX) were used to construct a half subtractor (Fig. S15a, Supporting Information). The high Cy3 fluorescence signal is defined as an output of (0,1), indicating that the BORROW (B) output is 0 and the DIFFERENCE (D) output is 1. The high ROX fluorescence signal is defined as an output of (1,1), indicating that the BORROW (B) output is 1 and the DIFFERENCE (D) output is 1. The high Cy5 fluorescence signal is defined as an output of (0,0), indicating that the BORROW (B) output is 0 and the DIFFERENCE (D) output is 0. In the half subtractor operation, an INHIBIT logic gate was used to carry out the BORROW bit function and a XOR logic gate was used to carry out the DIFFERENCE bit function. The logic circuit of the half subtractor was shown in Fig. 4f. The details of the DNA reaction process were shown in Fig. S15b (Supporting Information). The results of the half subtractor were shown in Fig. 4g,i. The (0,0) and (1,1) input combinations (A0B0 and A1B1) produce a high Cy5 fluorescence signal. The (0,1) input

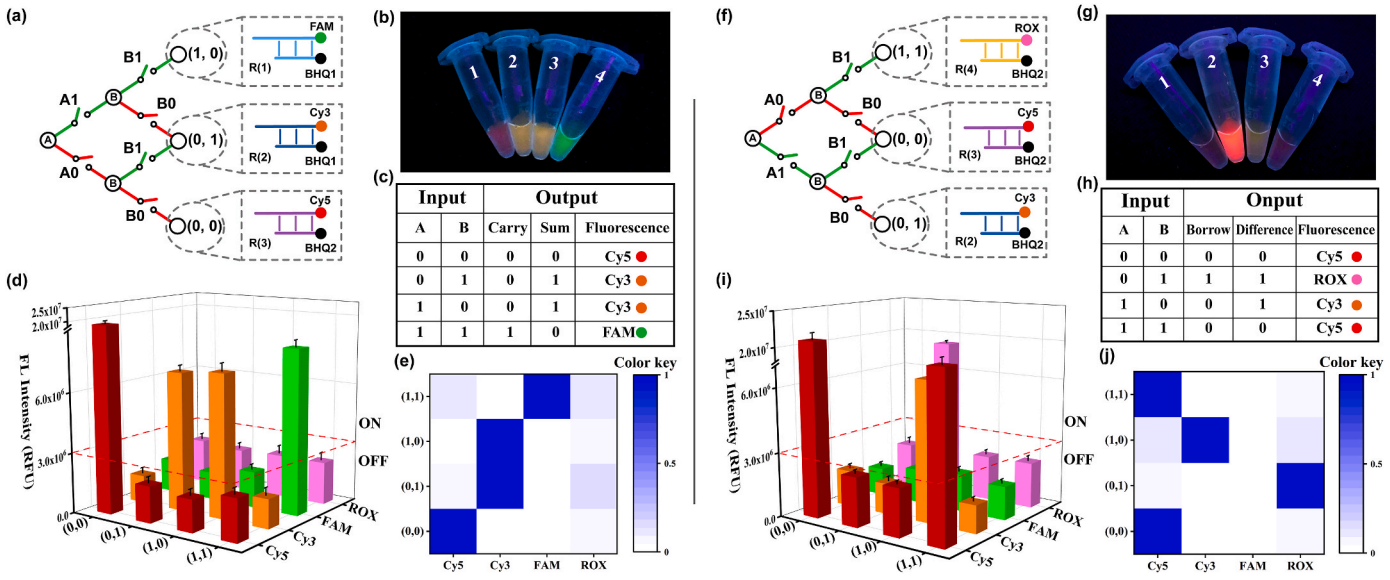

Fig. 4. Construction of half adder and half subtractor. (a) The MSs net of a half adder. (b) The fluorescence colors the half adder (the tubes 1–4 represent the input combinations of (0,0), (0,1), (1,0), and (1,1), respectively). (c) Truth table of the half adder. (d) Histogram shows the fluorescence intensities of the half adder. The red dashed line shows the threshold value of 3.0×10^6. (e) Heat map of logic fluorescence signals in half adder. (f) The MSs net of a half subtractor. (g) The fluorescence colors the half subtractor (the tubes 1–4 represent the input combinations of (0,0), (0,1), (1,0), and (1,1), respectively). (h) Truth table of the half subtractor. (i) Histogram shows the fluorescence intensities of the half subtractor. The red dashed line shows the threshold value of 3.0×10^6. (j) Heat map of logic fluorescence signals in the half subtractor.

combination (A0B1) produces a high ROX fluorescence signal. The (1,0) input combination (A1B0) produces a high Cy3 fluorescence signal. The truth table was shown in Fig. 4h. The heat map of the half adder results was shown in Fig. 4j. The circuit diagram of the half subtractor was shown in Fig. S16b (Supporting Information). The fluorescence kinetics data of the half subtractor were shown Fig. S16d (Supporting Information). The response of the half subtractor is rapid and can be finished within 6 min.

3.4. Construction of full adder and full subtractor

For full adder and full subtractor construction, another two MSs (switch 5 and switch 6) respond to switching signals C1 and C0 were added. C1 is the specific SARS-CoV-2 Lambda variant (C.37) sequence. C0 is the specific SARS-CoV-2 Omicron variant (B.1.1.529) sequence. The full adder can be realized by integrating two half adders and a OR logic gate (Fig. 5a). The switching signals A and B were used as the two inputs to activate the upstream half adder. The SUM (S) output from the upstream half adder (O_S in) and the switching signal C were used as the two inputs to activate the downstream half adder. The SUM (S) output of the downstream half adder was defined as the SUM (S) output (O_S) of the full adder. The CARRY (C) outputs from the two half adders were used as the two inputs to activate a OR logic gate. The output of the OR logic gate was defined as the CARRY (C) output (O_C) of the full adder. Four reporters (R(5), R(6), R(7) and R(8)) modified with four fluorophores (ROX, FAM, Cy3, and Cy5) were used to visualize the full adder (Fig. S19a, Supporting Information). The high ROX fluorescence signal is defined as an output of (1,1), indicating that the O_C is 1 and the O_S is 1. The high FAM fluorescence signal is defined as an output of (1,0), indicating that the O_C is 1 and the O_S is 0. The high Cy3 fluorescence signal is defined as an output of (0,1), indicating that the O_C is 0 and the O_S output is 1. The high Cy5 fluorescence signal is defined as an output of (0,0), indicating that the O_C is 0 and the O_S output is 0. The logic circuit of the full adder was shown in Fig. 5b. The details of the DNA reaction process were shown in Fig. S19b (Supporting Information). The results of the full adder were shown in Fig. 5c,e. The (0,0,0) input combination (A0B0C0) produces a high Cy5 fluorescence signal. The (0,0,1), (0,1,0), and (1,0,0) input combinations (A0B0C0, A0B1C0, and A1B0C0) produce a high Cy3 fluorescence signal. The (0,1,1), (1,0,1), and (1,1,0) input combinations (A0B1C1, A1B0C1, and A1B1C0) produces a high FAM fluorescence signal. The (1,1,1) input combination (A1B1C1) produces a high ROX fluorescence signal. The truth table of the full adder was shown in Fig. 5d. The heat map of the half adder results was shown in Fig. 5f. The circuit diagram of the full adder was shown in Fig. S20 (Supporting Information). The fluorescence kinetics data of the full adder were shown Fig. S22a (Supporting Information). The response of the full adder is rapid and can be finished within 10 min.

We further built a full subtractor by integrating two half subtractor and a OR logic gate (Fig. 5g). The switching signals A and B were used as the two inputs to activate the upstream half subtractor. The

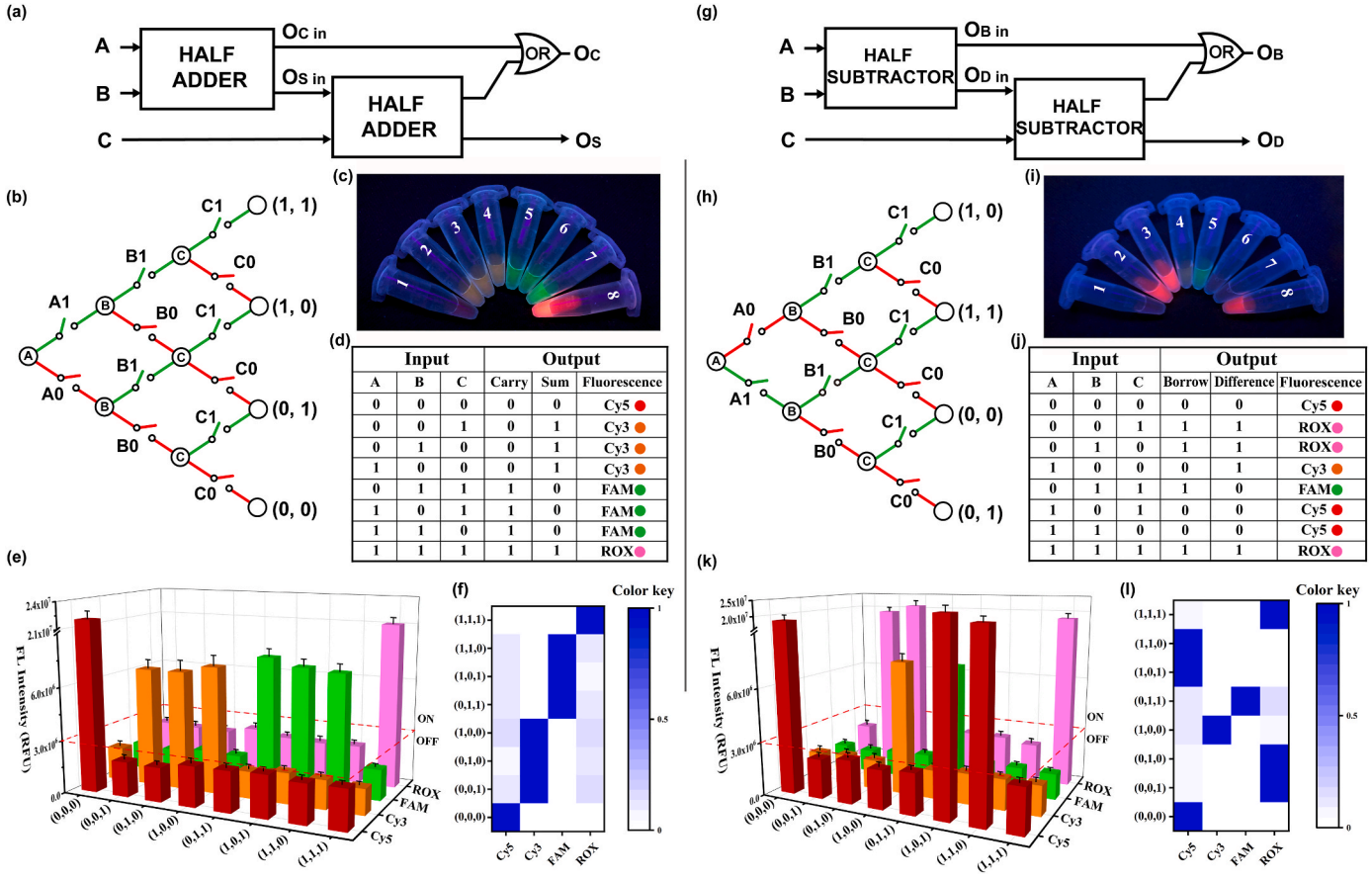

Fig. 5. Construction of full adder and full subtractor. (a) Assemble a full adder with two half adders and a OR logic gate. (b) The MSs net of the full adder. (c) The fluorescence colors the full adder (the tubes 1–8 represent the input combinations of (0,0,0), (0,0,1), (0,1,0), (1,0,0), (0,1,1), (1,0,1), (1,1,0), and (1,1,1), respectively). (d) Truth table of the full adder. (e) Histogram shows the fluorescence intensities of the full adder. The red dashed line shows the threshold value of 3.0×10^6. (f) Heat map of logic fluorescence signals in the full adder. (g) Assemble a full subtractor with two half subtractors and a OR logic gate. (h) The MSs net of a full subtractor. (i) The fluorescence colors the full subtractor (the tubes 1–8 represent the input combinations of (0,0,0), (0,0,1), (0,1,0), (1,0,0), (0,1,1), (1,0,1), (1,1,0), and (1,1,1), respectively). (j) Truth table of the full subtractor. (k) Histogram shows the fluorescence intensities of the full subtractor. The red dashed line shows the threshold value of 3.0×10^6. (l) Heat map of logic fluorescence signals in the full subtractor.

DIFFERENCE (D) output from the upstream half subtractor (O_D in) and the switching signal C were used as the two inputs to activate the downstream half subtractor. The DIFFERENCE (D) output of the downstream half subtractor was defined as the DIFFERENCE (D) output (O_D) of the full subtractor. The BORROW (B) outputs from the two half subtractors were used as the two inputs to activate a OR logic gate. The output of the OR logic gate was defined as the BORROW (B) output (O_B) of the full subtractor. Four reporters (R(5), R(6), R(7) and R(8)) modified with four fluorophores (ROX, FAM, Cy3, and Cy5) were used to construct a full subtractor (Fig. S21a, Supporting Information). The high Cy3 fluorescence signal is defined as an output of (0,1), indicating that the O_B is 0 and the OD is 1. The high ROX fluorescence signal is defined as an output of (1,1), indicating that the O_B and O_D are 1. The high Cy5 fluorescence signal is defined as an output of (0,0), indicating that the O_B and O_D are 0. The high FAM fluorescence signal is defined as an output of (1,0), indicating that the O_B is 1 and the O_D is 0. The logic circuit of the full subtractor was shown in Fig. 5h. The details of the DNA reaction process were shown in Fig. S21b (Supporting Information). The results of the full subtractor were shown in Fig. 5i,k. The (0,0,0), (1,0,1), and (1,1,0) input combination (A0B0C0, A1B0C1, and A1B1C0) produce a high Cy5 fluorescence signal. The (0,0,1), (0,1,0), and (1,1,1) input combinations (A0B0C0, A0B1C0, and A1B1C1) produce a high ROX fluorescence signal. The (1,0,0) input combination (A1B0C0) produces a high Cy3 fluorescence signal. The (0,1,1) input combination (A0B1C1) produces a high FAM fluorescence signal. The truth table of the full subtractor was shown in Fig. 5j. The heat map of the half subtractor results was shown in Fig. 5l. The circuit diagram of the full subtractor was shown in Fig. S20 (Supporting Information). The fluorescence kinetics data of the full subtractor were shown Fig. S22b (Supporting Information). The response of the full subtractor is rapid and can be finished within 10 min. We summarized a table to compare the sensing performance of our DNA biocomputing circuit with some previously reported methods for SARS-CoV-2 detection (Table S2, Supporting Information). An important merit of our logic sensor is that the logic gate system can realize the intelligent screening of six SARS-CoV-2 variants by the naked eye within 10 min.

3.5. Real sample analysis

With the continuous mutation of the SARS-CoV-2 and the success of epidemic prevention and control, the real samples of the Beta (B.1.351), Delta (B.1.617.2), Kappa (B.1.617.1), Lambda (C.37), and Omicron (B.1.1.529) variants are very scarce. To assess the practical performance of MSs net in real samples, a recovery experiment was carried out by operating a full adder in mouth saliva samples. The mouth saliva samples were collected from healthy people, and filtered through a 0.22 μm membrane to remove the insoluble particles. The specific variant sequences of A1, A0, B1, B0, C1, and C0 were spiked in the saliva samples to execute the full adder. As shown in Fig. S23 (Supporting Information), the full adder can work effectively even in real saliva samples. The (0,0,0) input combination (A0B0C0) produces a high Cy5 fluorescence signal. The (0,0,1), (0,1,0), and (1,0,0) input combinations (A0B0C0, A0B1C0, and A1B0C0) produce a high Cy3 fluorescence signal. The (0,1,1), (1,0,1), and (1,1,0) input combinations (A0B1C1, A1B0C1, and A1B1C0) produces a high FAM fluorescence signal. The (1,1,1) input combination (A1B1C1) produces a high ROX fluorescence signal. Those results indicated that our proposed logic system is robust and the complex sample matrices do not interfere with the assay results. Such reliable sensing capabilities enable the MSs net to be developed as an ideal large-scale screening tool for the monitoring of SARS-CoV-2 variants in real samples.

4. Conclusion

In conclusion, we have successfully fabricated several logic systems (NOT, AND, OR, INHIBIT, XOR, half adder, half subtractor, full adder, and full subtractor) for the intelligent sensing of SARS-CoV-2 variants based on different MSs interactions. SARS-CoV-2 and several variants, including Beta (B.1.351), Delta (B.1.617.2), Kappa (B.1.617.1), Lambda (C.37), and Omicron (B.1.1.529) were used as the inputs to activate the logic functions. Through multichannel logic operations, we can simultaneously distinguish different variants using four fluorophores (FAM, Cy3, ROX, and Cy5) as the output signals. The logic response is fast and we can get the results within 10 min, which is in favor of the rapid screening of SARS-CoV-2 variants. The operation of the logic system is simple and the logic results can be directly observed by the naked-eye under a portable UV lamp. The output of biocomputing circuits is still accurate and reliable in the presence of various variants, demonstrating that the system is competent for intelligent wide-population screening of SARS-CoV-2 variants. With the advantages of rapid response, simple operation, multichannel analysis, and intuitive outputs, our developed logic system can realize the intelligent point-of-care screening of SARS-CoV-2 variants without the requirement of any sophisticated instrumental techniques.

CRediT authorship contribution statement

Fang Deng: Conceptualization, Methodology, Data curation, Writing – original draft. **Jiafeng Pan:** Methodology, Validation, Formal analysis. **Zhi Liu:** Methodology, Data curation, Validation. **Lingwen Zeng:** Methodology, Formal analysis, Funding acquisition. **Junhua Chen:** Conceptualization, Funding acquisition, Project administration, Supervision, Writing – review & editing.

Declaration of competing interest

The authors declare that they have no known competing financial interests or personal relationships that could have appeared to influence the work reported in this paper.

Data availability

Data will be made available on request.

Acknowledgment

This work was supported by the Guangdong Basic and Applied Basic Research Foundation (2021A1515012192 and 2019B1515210019), Foshan Science and Technology Innovation Team Project (2018IT100343), Wuhan Science and Technology Plan Project (2020030603012347), and the Key Research and Development Projects of Hubei Province (2020BBA053).

Appendix A. Supplementary data

Supplementary data to this article can be found online at https://doi.org/10.1016/j.bios.2022.115025.

References

Arter, W.E., Yusim, Y., Peter, Q., Taylor, C.G., Klenerman, D., Keyser, U.F., Knowles, T.P. J., 2020. ACS Nano 14, 5763–5771.
Bai, C., Wang, J., Chen, G., Zhang, H., An, K., Xu, P., Du, Y., Ye, R.D., Saha, A., Zhang, A., Warshel, A., 2021. J. Am. Chem. Soc. 143, 17646–17654.
Cai, Z., Wang, A., Wang, Y., Qiu, Z., Li, Y., Yan, H., Fu, M., Liu, M., Yu, Y., Gao, F., 2022. Anal. Chem. 94, 9715–9723.
Cevik, M., Tate, M., Lloyd, O., Maraolo, A.E., Schafers, J., Ho, A., 2021. Lancet Microbe 2, e13–e22.
Chen, J., Chen, S., Li, F., 2018. Anal. Chem. 90, 10311–10317.
Chen, J., Fang, Z., Lie, P., Zeng, L., 2012. Anal. Chem. 84, 6321–6325.
Chen, Y., Gong, X., Gao, Y., Shang, Y., Shang, J., Yu, S., Li, R., He, S., Liu, X., Wang, F., 2021. Chem. Sci. 12, 15710–15718.
Cyranoski, D., 2021. Nature 589, 337–338.
Dai, C., Liu, Y., Wei, D., 2021. Chem. Rev. 122, 10315–10392.
Erdem, Ö., Eş, I., Saylan, Y., Inci, F., 2022. Anal. Chem. 94, 3–25.

Feng, C., Chen, T., Mao, D., Zhang, F., Tian, B., Zhu, X., 2020. ACS Sens. 5, 3116–3123.
Feng, W., Newbigging, A.M., Tao, J., Cao, Y., Peng, H., Le, C., Wu, J., Pang, B., Li, J., Tyrrell, D.L., Zhang, H., Le, X.C., 2021. Chem. Sci. 12, 4683–4698.
Garg, S., Shah, S., Bui, H., Song, T., Mokhtar, R., Reif, J., 2018. Small 14, 1801470.
Ge, L., Wang, W.X., Sun, X.M., Hou, T., Li, F., 2016. Anal. Chem. 88, 9691–9698.
Gong, X., Wei, J., Liu, J., Li, R., Liu, X., Wang, F., 2019. Chem. Sci. 10, 2989–2997.
Goswami, S., Pramanick, R., Patra, A., Rath, S.P., Foltin, M., Ariando, A., Thompson, D., Venkatesan, T., Goswami, S., Williams, R.S., 2021. Nature 597, 51–56.
Han, Y., Yang, Z., Hu, H., Zhang, H., Chen, L., Li, K., Kong, L., Wang, Q., Liu, B., Wang, M., Lin, J., Chen, P.R., 2022. J. Am. Chem. Soc. 144, 5702–5707.
Hao, Z., Yan, Y., Shi, Y., Li, Y., 2022. J. Phys. Chem. Lett. 13, 1914–1924.
Kaminski, M.M., Abudayyeh, O.O., Gootenberg, J.S., Zhang, F., Collins, J.J., 2021. Nat. Biomed. Eng. 5, 643–656.
Lee, M., Jeon, Y., Moon, T., Kim, S., 2011. ACS Nano 5, 2629–2636.
Liang, Y., Lin, H., Zou, L., Deng, X., Tang, S., 2022. Biosens. Bioelectron. 205, 114098.
Li, J., Lai, S., Gao, G.F., Shi, W., 2021. Nature 600, 408–418.
Moitra, P., Chaichi, A., Hasan, S.M.A., Dighe, K., Alafeef, M., Prasad, A., Gartia, M.R., Pan, D., 2022. Biosens. Bioelectron. 208, 114200.
Qian, L., Winfree, E., 2011. Science 332, 1196–1201.
Rahimi, H., Salehiabar, M., Barsbay, M., Ghaffarlou, M., Kavetskyy, T., Sharafi, A., Davaran, S., Chauhan, S.C., Danafar, H., Kaboli, S., Nosrati, H., Yallapu, M.M., Conde, J., 2021. ACS Sens. 6, 1430–1445.
Rockett, R.J., Draper, J., Gall, M., Sim, E.M., Arnott, A., Agius, J.E., Mackinnon, J.J., Fong, W., Martinez, E., Drew, A.P., Lee, C., Ngo, C., Ramsperger, M., Ginn, A.N., Wang, Q., Fennell, M., Ko, D., Hueston, L., Kairaitis, L., Holmes, E.C., O'Sullivan, M. N., Chen, S.C.A., Kok, J., Dwyer, D.E., Sintchenko, V., 2022. Nat. Commun. 13, 2745.
Rodriguez, J., Malpartida, K., Moser, N., Pennisi, I., Cavuto, M., Miglietta, L., Moniri, A., Penn, R., Satta, G., Randell, P., Davies, F., Bolt, F., Barclay, W., Holmes, A., Georgiou, P., 2021. ACS Cent. Sci. 7, 307–317.
Song, T., Eshra, A., Shah, S., Bui, H., Fu, D., Yang, M., Mokhtar, R., Reif, J., 2019. Nat. Nanotechnol. 14, 1075–1081.
Su, H., Xu, J., Wang, Q., Wang, F., Zhou, X., 2019. Nat. Commun. 10, 5390.
Sun, X., Yi, C., Zhu, Y., Ding, L., Xia, S., Chen, X., Liu, M., Gu, C., Lu, X., Fu, Y., Chen, S., Zhang, T., Zhang, Y., Yang, Z., Ma, L., Gu, W., Hu, G., Du, S., Yan, R., Fu, W., Yuan, S., Qiu, C., Zhao, C., Zhang, X., He, Y., Qu, A., Zhou, X., Li, X., Wong, G., Deng, Q., Zhou, Q., Lu, H., Ling, Z., Ding, J., Lu, L., Xu, J., Xie, Y., Sun, B., 2022. Nat. Microbiol. 7, 1063–1074.
Suzuki, R., Yamasoba, D., Kimura, I., Wang, L., Kishimoto, M., Ito, J., Morioka, Y., Nao, N., Nasser, H., Uriu, K., Kosugi, Y., Tsuda, M., Orba, Y., Sasaki, M., Shimizu, R., Kawabata, R., Yoshimatsu, K., Asakura, H., Nagashima, M., Sadamasu, K., Yoshimura, K., , Genotype to Phenotype Japan (G2P-Japan) Consortium, Sawa, H., Ikeda, T., Irie, T., Matsuno, K., Tanaka, S., Fukuhara, T., Sato, K., 2022. Nature 603, 700–705.
Syeda, A.M., Ciling, A., Taha, T.Y., Chen, I.P., Khalid, M.M., Sreekumar, B., Chen, P.Y., Kumar, G.R., Suryawanshi, R., Silva, I., Milbes, B., Kojima, N., Hess, V., Shacreaw, M., Lopez, L., Brobeck, M., Turner, F., Spraggon, L., Tabata, T., Ott, M., Doudna, J.A., 2022. Proc. Natl. Acad. Sci. U.S.A. 119, e2200592119.
Valera, E., Jankelow, A., Lim, J., Kindratenko, V., Ganguli, A., White, K., Kumar, J., Bashir, R., 2021. ACS Nano 15, 7899–7906.
Wang, C., Horby, P.W., Hayden, F.G., Gao, G.F., 2020a. Lancet 395, 470–473.
Wang, F., Lv, H., Li, Q., Li, J., Zhang, X., Shi, J., Wang, L., Fan, C., 2020b. Nat. Commun. 11, 121.
Wang, Y., Zhang, Y., Chen, J., Wang, M., Zhang, T., Luo, W., Li, Y., Wu, Y., Zeng, B., Zhang, K., Deng, R., Li, W., 2021. Anal. Chem. 93, 3393–3402.
Xiong, E., Jiang, L., Tian, T., Hu, M., Yue, H., Huang, M., Lin, W., Jiang, Y., Zhu, D., Zhou, X., 2021. Angew. Chem. Int. Ed. 60, 5307–5315.
Yang, K., Schuder, D.N., Ngor, A.K., Chaput, J.C., 2022. J. Am. Chem. Soc. 144, 11685–11692.
Yao, L., Zhu, W., Shi, J., Xu, T., Qu, G., Zhou, W., Yu, X.F., Zhang, X., Jiang, G., 2021. Chem. Soc. Rev. 50, 3656–3676.
Zhou, P., Yang, X.L., Wang, X.G., Hu, B., Zhang, L., Zhang, W., Si, H.R., Zhu, Y., Li, B., Huang, C.L., Chen, H.D., Chen, J., Luo, Y., Guo, H., Jiang, R.D., Liu, M.Q., Chen, Y., Shen, X.R., Wang, X., Zheng, X.S., Zhao, K., Chen, Q.J., Deng, F., Liu, L.L., Yan, B., Zhan, F.X., Wang, Y.Y., Xiao, G.F., Shi, Z.L., 2020. Nature 579, 270–273.
Zhang, C., Zhao, Y., Xu, X., Xu, R., Li, H., Teng, X., Du, Y., Miao, Y., Lin, H., Han, D., 2020. Nat. Nanotechnol. 15, 709–715.
Zhang, W., Liu, N., Zhang, J., 2022. Biosens. Bioelectron. 201, 113944.